

Illuminating dark objects with dark matter lampshades

Joseph Bramante^{1,2,3,*}, Melissa D. Diamond^{1,2,3,†} and J. Leo Kim^{1,2,‡}

¹*Department of Physics, Engineering Physics, and Astronomy,
Queen's University, Kingston, Ontario, K7L 3N6, Canada*

²*Arthur B. McDonald Canadian Astroparticle Physics Research Institute,
Kingston ON K7L 3N6, Canada*

³*Perimeter Institute for Theoretical Physics, Waterloo, ON N2J 2W9, Canada*

We demonstrate a new technique to search for dark compact objects. When dark matter comprising a dark compact object interacts with photons, the compact object can disperse light traveling through it. As these objects pass between the Earth and a distant star, they act as “lampshades” that dim the star. We examine how dimming effects from clumps of dark matter in the galaxy could be searched for in microlensing surveys, which measure the brightness of stars as a function of time. Using the EROS-2 and OGLE surveys, we show that a dimming analysis of existing data can be used to constrain dark sectors, and could be used to discover dark matter in compact objects.

I. INTRODUCTION

Primordial black holes (PBHs) [1, 2] and MAssive Compact Halo Objects (MACHOs) are of prominent interest for beyond-Standard Model (BSM) studies of the Universe, both as dark matter (DM) candidates (see, e.g., Refs. [3–5]) and as natural consequences of many self-interacting dark sectors and exotic cosmologies [6–24]. There are several ways to observe and constrain these objects [25–34]. Prominent among these are microlensing [35] searches, which look for the amplification of starlight from a bright source due to gravitational lensing from an intermediate heavy object. Over the last several years, microlensing surveys, such as EROS-2 [36], OGLE [37, 38], and Subaru/HSC [39], have played an essential role in the hunt for BSM physics – providing some of the most sensitive probes of PBHs and MACHOs in the $10^{-10}M_{\odot}$ to $10M_{\odot}$ mass range [40].

Microlensing searches need not be limited to observing the heavy point-like objects they traditionally look for. Recent works have studied how existing microlensing constraints are significantly altered if one considers an extended dark matter structure rather than a point-like object for both point sources [41] and extended sources [42]. For a collection of constraints on extended dark matter objects, see Ref. [43].

However, the data from these surveys can also be used search for objects that are too light or too diffuse to observably microlense a source star. Dark sector compact objects which have weak interactions with the Standard Model (SM) can scatter starlight. As a result, when the DM objects pass between Earth and the source stars, they can act as “lampshades”, dimming the source starlight. Microlensing surveys, which are sensitive to slight changes in the brightness of distant stars as a function of time are well equipped to look for this dimming.

Excitingly, these dimming effects are most observable for objects microlensing surveys are not otherwise sensitive to, broadening the scope of what they can observe.

In this work, we study the dimming effects of starlight due to diffuse, self-gravitating clouds of dark matter which interact with SM photons. The idea is similar to Ref. [44], which studied the dimming of starlight similar to exoplanet searches, where in [44] this required that dark exoplanets would be gravitationally bound to the source star. Here we will consider free-floating structures of DM in the galaxy, which can enter the observing tube anywhere between the source star and a local observer. In particular, we modify the previously existing formalism [45, 46] for microlensing events to account for dimming events, by defining a dimming event as a drop in apparent magnitude, and by replacing the Einstein radius of the object with the physical radius of the object.

We demonstrate the sensitivity of the microlensing surveys for dimming effects, which is summarized in Fig. 1. As the amount of dimming is dependent on the SM photon-DM interaction, we first show how dimming effects could constrain a general cross section and the mass of the DM particle that make up the compact structure. We then choose a specific DM model – millicharged dark matter [47] – to show how dimming effects could be used to place complementary constraints on the specific model parameters. Assuming they reside in compact objects, we show that there are competitive bounds that could be placed on millicharged particles, using null observations of dimming events. For this work, we will remain agnostic about the formation mechanism for these dark compact objects, although recently many mechanisms have been identified for MACHO formation in the early universe [6–24].

This paper is structured as follows. In Section II we define an event for the dimming of starlight due to clouds of DM assuming point sources. In Section III we present event rates for these dimming events, and show where several different microlensing surveys would be sensitive to these effects, and also show how dimming events could be used to place constraints on macrophysical DM properties, such as the amount of DM in clumps of a cer-

* joseph.bramante@queensu.ca

† m.diamond@queensu.ca

‡ leo.kim@queensu.ca

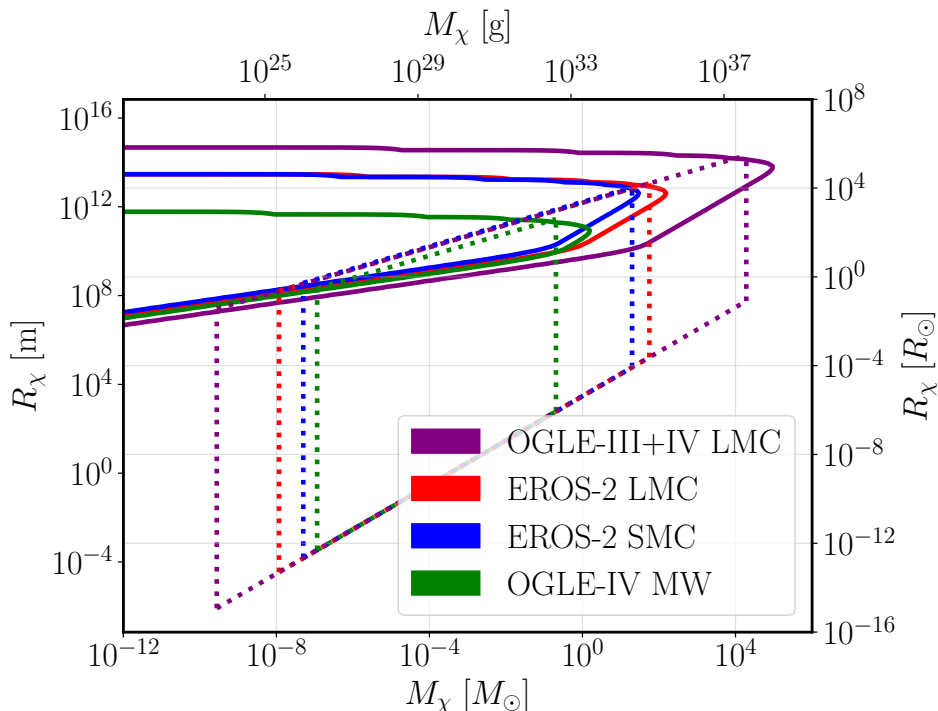


FIG. 1. Heuristic plot showing the sensitivity of the microlensing surveys to dark matter clumps assuming that $R_{\chi,\text{eff}} \approx R_{\chi}$. The region enclosed inside of the solid curves are where the surveys are sensitive to dimming effects, whereas the region inside of the dashed lines are where the surveys are sensitive to microlensing [41].

tain size and mass. Section IV demonstrates how the null observation of dimming events in microlensing surveys can be mapped onto constraints on microscopic DM properties, such as DM mass, SM-DM cross section, and specific model parameters in millicharged DM. Section V concludes.

II. DIMMING EVENT FROM DARK MATTER LAMPSHADES

To determine stellar dimming by dark matter objects, we begin by assuming that a source star is a point source and consider an extended spherical dark matter cloud with constant density ρ_{χ} and physical radius R_{χ} . The transmittance (*i.e.* the amount of star light that passes through the DM cloud) at a position a distance r from the center of the cloud is given by

$$T(r) = \exp\left(-2\tau_0\sqrt{1 - (r/R_{\chi})^2}\right), \quad (1)$$

where

$$\tau_0 \equiv R_{\chi}n_{\chi}\sigma, \quad (2)$$

is the characteristic optical depth of the DM cloud. The cross section σ pertains to the interactions between dark matter particles and photons that causes the dimming, and $n_{\chi} = \rho_{\chi}/m_{\chi}$ is the number density of the χ particles

in the DM cloud. The maximum dimming effect occurs when a light ray traverses the full diameter $2R_{\chi}$ through the centre of the DM cloud at $r = 0$, so that $T(0) = e^{-2\tau_0}$. In order to trigger a dimming event, we require a minimum fraction μ_0 of light blocked by the cloud. The effective radius at which this occurs is

$$R_{\chi,\text{eff}} = R_{\chi}\sqrt{1 - \frac{1}{4\tau_0^2}[\ln(1 - \mu_0)]^2}. \quad (3)$$

The multiplicative factor on the right-hand side of Eq. (3) is analogous to the usual impact parameter u_T in the case of microlensing [45]. In our case, we consider a compact object transit is able to produce a detectable dimming event if, tracking the star's path behind the DM clump, the background source passes within $R_{\chi,\text{eff}}$ of the center of the DM sphere. Note that Eq. (3) gives a minimum value of τ_0 to get a real solution, which is given by

$$\tau_{0,\text{min}} = \frac{1}{2}\ln(1 - \mu_0). \quad (4)$$

Therefore, if a dimming event occurs, the measured flux of the source star is diluted to a fraction $1 - \mu_0 = 10^{(\bar{m} - m_{\text{dim}})/2.5}$, where m_{dim} is the dimmed apparent magnitude and \bar{m} is the fiducial apparent magnitude of the source.

The relationship between the effective radius of the cloud in terms of its physical radius, and the cloud's characteristic optical depth is shown in Fig. 2, which shows

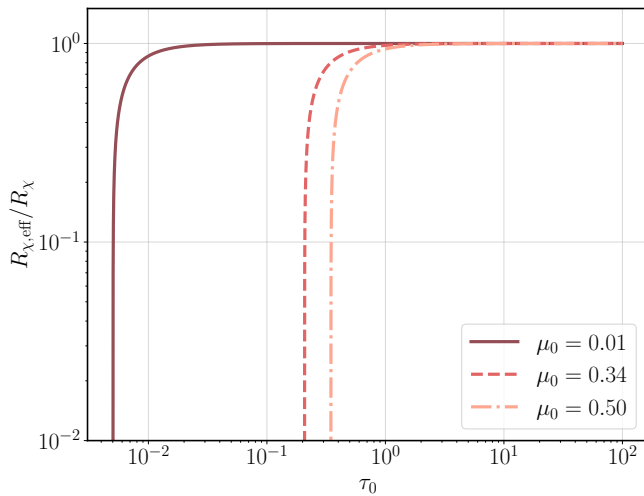


FIG. 2. The effective radius $R_{\chi, \text{eff}}$ at which the source star is dimmed by a fraction μ_0 as a function of the characteristic optical depth τ_0 . The solid, dashed, and dotted-dashed curves correspond to effective radii assuming $\mu_0 = 0.01, 0.34$, and 0.50 respectively.

the effective radius as a function of optical depth for three different values of μ_0 . For a given value of the characteristic optical depth τ_0 , the size of the DM cloud can be determined by the dip in magnitude. In microlensing surveys, for an event to be registered, the total amplification must exceed a threshold, given conventionally by $\mu_T = 1.34$ [35] – *i.e.* a 34% amplification. While a convention has not been established for dimming, we choose $\mu_0 = 0.34$ as the fiducial value throughout this paper so that a dimming event occurs when 34% of the starlight is dimmed. If a fiducial value of $\mu_0 = 0.34$ is selected, then we see that $R_{\chi, \text{eff}} \approx R_{\chi}$ for $\tau_0 \geq 1$. In what follows, we will work with $\tau_0 = 1$ unless otherwise stated.

III. DIMMING EVENT RATES

To model the dimming event rates, we follow a procedure similar to past microlensing treatments [41, 42], with modifications necessary for dimming. We assume all dark matter clumps have a mass M_{χ} , and velocities set by a Maxwell-Boltzmann distribution. We assume that the line-of-sight density of clumps in the galaxy is given by $\rho_{\text{clumps}}(x) = f_{\text{DM}}\rho_{\text{DM}}(x)$, where f_{DM} is the fraction of dark matter residing in these clumps and ρ_{DM} is the position-dependent dark matter density. Note that we have used the conventional variable $x = D_L/D_S$ to parameterize distances, where D_L is the distance to the clump (normally the gravitational lens in microlensing scenarios), and D_S is the distance to the source field. For simplicity, the dark matter density for the Milky Way (MW) is modelled assuming an isothermal profile

$$\rho_{\text{DM}}(r(x)) = \frac{\rho_s}{1 + (r(x)/r_s)^2}, \quad (5)$$

where $r_s = 4.38$ kpc is the central scale radius, and

$$r(x) = \sqrt{R_{\text{Sol}}^2 - 2xR_{\text{Sol}}D_S \cos \ell \cos b + x^2D_S^2}, \quad (6)$$

in which $R_{\text{Sol}} = 8.5$ kpc is the distance to the sun and $\rho_s = 1.39$ GeV/cm³ is the central density [52]. The differential event rate for microlensing events is given by [45, 46]

$$\frac{d^2\Gamma}{dxdt_E} = \varepsilon(t_E) \frac{2D_S}{v_0^2 M_{\chi}} f_{\text{DM}} \rho_{\text{DM}}(x) v_E^4(x) e^{-v_E^2(x)/v_0^2}, \quad (7)$$

where $v_0 = 220$ km/s is the circular speed of DM in our galaxy, v_E is the relative velocity of the lensing system for the duration of the event, and $\varepsilon(t_E)$ is the so-called efficiency parameter. In this work we take a constant value of $\varepsilon(t_E) = 1$, as evaluating the efficiency parameter for dimming is outside the scope of this study. Given this rate, the associated number of events can be expressed as

$$N_{\text{events}} = N_* T_{\text{obs}} \int_0^1 dx \int_{t_{E, \text{min}}}^{t_{E, \text{max}}} dt_E \frac{d^2\Gamma}{dxdt_E}, \quad (8)$$

where $t_{E, \text{min}}$ ($t_{E, \text{max}}$) is the minimum (maximum) timescale that the survey is sensitive to, N_* is the number of stars in the source field, and T_{obs} is the total observing time of the survey. Appendix B of Ref. [41] has shown that the integral in Eq. (8) can be efficiently computed, since the integral over t_E has an analytical solution. In this work we evaluate the integral according to

$$A \int dt_E \frac{e^{-B/t_E^2}}{t_E^4} = \frac{A}{2B} \left[\frac{e^{-B/t_E^2}}{t_E} - \frac{\sqrt{\pi} \operatorname{erf}(\sqrt{B}/t_E)}{\sqrt{B}} \right], \quad (9)$$

which we include here for completeness.

Next we note that $t_{E, \text{min}}$ and $t_{E, \text{max}}$ are determined by the behaviour of their respective efficiency parameters, which are in turn related to the observing cadence and total observation time of the detector. Here we will use the minimum and maximum event times computed by the microlensing surveys [36, 48–50], except for OGLE-III+IV, where we have taken $t_{E, \text{max}} = 7300$ days (corresponding to 20 years) rather than the 10000 days the analysis was performed up to. Although the event rate and count were originally conceived for microlensing events, these expressions can be easily recasted for dimming effects. The primary difference comes from considering the physical radii of the clumps rather than their Einstein radii. In this case, the quantity v_E is given by

$$v_E = \frac{2R_{\chi, \text{eff}}}{t_E}, \quad (10)$$

where a key difference between Eq. (10) and the definition of v_E in Refs. [41, 42] is that in the case of microlensing, $v_E = 2(4GM_{\chi}D_Sx(1-x))^{1/2}/t_E$, which makes use

Survey	Source	$(D_S$ [kpc], ℓ , b)	N_*	T_{obs} [days]	t_E [days]
EROS-2 [36]	LMC	$(50, 280.46^\circ, -32.89^\circ)$	5.49×10^6	2500	[1, 1000]
	SMC	$(60, 302.81^\circ, -44.33^\circ)$	0.86×10^6		
OGLE-IV [48]	MW	$(8.5, 1.09^\circ, -2.39^\circ)$	4.88×10^7	1826	[0.1, 300]
OGLE-III+IV [49, 50]	LMC	$(50, 280.46^\circ, -32.89^\circ)$	7.87×10^7	7300	[1, 7300]

TABLE I. Table of characteristic information of microlensing surveys used for Fig. 1, modified from Ref. [41] which used data from Ref. [51], with additional data pertaining to OGLE-III+IV [49, 50].

of the Einstein radius rather than the physical size of the clump.

We consider four source fields in our analysis: the EROS-2 surveys of the Large Magellanic Cloud (LMC) and the Small Magellanic Cloud (SMC) [36], the 5-year dataset¹ from the OGLE-IV survey of the Milky Way bulge [48], and the 20-year dataset from the combined OGLE-III [37] and OGLE-IV [38] (henceforth OGLE-III+IV) surveys of the LMC [49, 50]. The necessary information regarding the survey parameters required for the event rate is summarized in Table I. We have taken the relevant values for EROS-2 and OGLE-IV from Ref. [41] and adopted parameters from Refs. [49, 50] for OGLE-III+IV. Note that for simplicity, we have considered the same range of event times for dimming events as previous microlensing studies.

As already mentioned, Fig. 1, which can be compared to microlensing mass reach figures in Refs. [41, 42], shows a heuristic estimate of the masses M_χ and physical radii R_χ of spherical DM clumps which can be probed using the EROS-2, OGLE-IV, and OGLE-III+IV² microlensing surveys. To demonstrate the sensitivity of a survey to dimming and microlensing events, all enclosed regions have at least one event following Eq. (8). The regions enclosed by the solid curves are where the surveys are sensitive to dimming effects, while the regions enclosed by dotted lines are where the surveys would be sensitive to microlensing. Note that the region for sensitivity for microlensing presented in Fig. 1 is different from that shown in Ref. [41], since we are considering a detection efficiency of $\varepsilon(t_E) = 1$ for both microlensing and dimming to present a fair comparison between “best-case” scenarios. We have also used full observation event time ranges

for microlensing presented in Table I instead of a range where the efficiency parameter was roughly constant, as in Ref. [41].

For microlensing surveys, the lower limit on the size of the object comes from the Schwarzschild radius $R_S = 2GM_\chi$ for a given cloud mass, while the upper limit is a result of the maximum Einstein radius which occurs at $x = 1/2$, so that $R_{E,\text{max}} = (GM_\chi D_S)^{1/2}$. Hence for a given clump mass, the surveys are more sensitive to microlensing at smaller sizes while at larger sizes they are more sensitive to dimming, which does not depend on the Einstein radius. In contrast, we see that the dimming effect not only allows for larger clumps to be found, between $10^{-2}R_\odot$ and 10^6R_\odot depending on the survey, but also lower masses in that range, since the physical radius is not fundamentally a function of the mass of the cloud. Rather, the relationship between the size of the object and its mass is dependent on the density profile of the object.

On that note, while Figure 1 indicates dimming sensitivity for arbitrarily small clump masses, in practice there will be a lower cutoff in M_χ for the sensitivity region. This will occur when the clump does not have enough material to observably dim starlight, which will depend on the density profile of the object as well as the chosen interaction between the SM photon and the DM particles inside the clump. Without specifying an explicit relationship for a density profile between M_χ and R_χ , the number of events, N_{events} , will continue to increase as M_χ decreases due to there being more clumps *cf.* Eq.(7). Note that in Fig. 1, we are assuming that the effective dimming radius is equal to the clump radius. $R_{\chi,\text{eff}} \approx R_\chi$, to demonstrate the best-case scenario for sensitivity to dimming effects.

In the work that follows, for simplicity, we will consider a constant density clump profile, so that $M_\chi = 4\pi\rho_\chi R_\chi^3/3$. In that case, the radius of the DM clump is given by

$$R_\chi = \sqrt{\frac{3}{4\pi} \frac{\sigma M_\chi}{m_\chi \tau_0}}. \quad (11)$$

With this assumption, N_{events} no longer monotonically decreases as a function of M_χ , and so a minimum mass can be obtained. Fig. 3 shows limits on the fraction of dark matter f_{DM} that could reside in dark matter clumps. To compute these limits on f_{DM} , we have taken $N_{\text{thresh}} = 3.9$ events as the threshold number of events required for a 90% confidence level observation of a sin-

¹ While there is an 8-year dataset for the OGLE-IV survey of the Milky Way bulge [53], we have used the 5-year dataset for comparison with Ref. [41] and also since any constraints from the 8-year dataset will be weaker than the 20-year OGLE-III+IV dataset of the LMC.

² Note that here we have only considered dimming events in the LMC due to DM clumps in the MW. However, there are also events expected from clumps in the LMC, which were considered in Refs. [49]. We find that events due to clumps from the LMC were always subdominant to those from the MW, improving the number of events at most by a factor of two, which agrees with the results found in Ref. [49], in which the number of events were dominated by MW objects except at small clump masses. For simplicity, we do not consider the additional events from clumps in the LMC, noting that these would strengthen the sensitivity/constraints shown, as they imply more events.

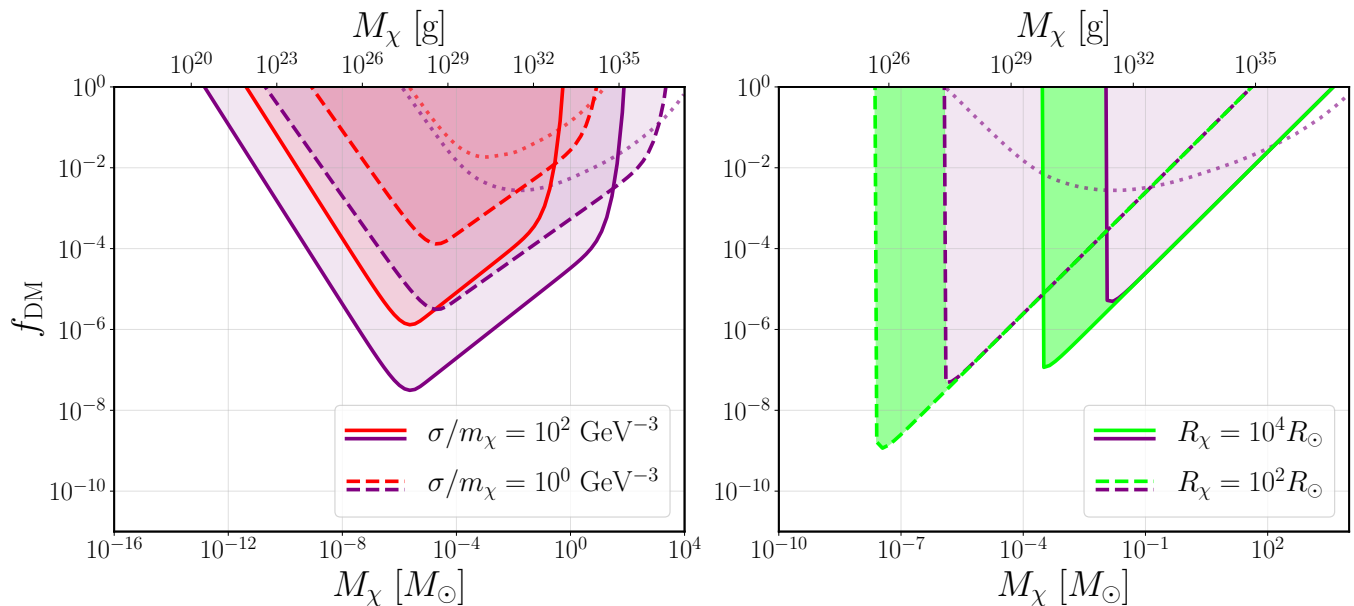


FIG. 3. **Left panel:** Limits on the fraction of dark matter f_{DM} inside clumps of mass M_χ assuming null observations of dimming effects in microlensing surveys, assuming a fixed characteristic optical depth of $\tau_0 = 1$. The red (purple) shaded areas correspond to restrictions on f_{DM} from the EROS-2 LMC (OGLE-III+IV) survey, with sizes R_χ computed from Eq. (11) at fixed values of σ/m_χ . The dotted curves in red and purple show restrictions on f_{DM} assuming microlensing from point sources from EROS-2 LMC [41] and OGLE-III+IV [49, 50], respectively. **Right panel:** Limits on the fraction of dark matter f_{DM} inside clumps of mass M_χ of fixed sizes of $R_\chi = 10^4 R_\odot$ in solid curves and $R_\chi = 10^2 R_\odot$ in dashed curves, assuming null observations of dimming effects in OGLE-III+IV. The regions enclosed and shaded in purple are assuming a dimming of $\mu_0 = 0.34$, while the lime green regions are where a dimming of $\mu_0 = 0.01$ was assumed. We have fixed $\sigma/m_\chi = 10^2 \text{ GeV}^{-3}$. The dotted curves in purple shows restrictions on f_{DM} assuming microlensing from point sources from OGLE-III+IV [49, 50].

gle event, following Poisson statistics [41]. The regions shaded above the curves displayed in Fig. 3 indicate $N_{\text{events}} \geq N_{\text{thresh}}$, where null observations of dimming events in the EROS-2 LMC and OGLE-III+IV surveys could be used to set constraints for a fraction of DM, f_{DM} , at a given DM clump mass. We have also plotted constraints on f_{DM} from point-like lenses in EROS-2 [42] and OGLE-III+IV [49, 50] in dotted curves.

In more detail, the left panel of Fig. 3 shows constraints on f_{DM} for two different values of σ/m_χ , for a fixed characteristic optical depth of $\tau_0 = 1$ so that $R_{\chi,\text{eff}} \approx R_\chi$, where R_χ was computed using Eq. (11). We have shown both EROS-2 LMC constraints in red and OGLE-III+IV LMC constraints in purple for comparison. Having a longer total observation time and a larger number of source stars allows one to limit f_{DM} to lower values, while having a longer maximum event time $t_{E,\text{max}}$ allows for access to higher clump masses due to the $R_\chi \propto M_\chi^{1/2}$ relationship in Eq. (11).

Alternatively, rather than fixing τ_0 and computing R_χ , one can also fix R_χ and solve for τ_0 using Eq. (11). This value of τ_0 can then be used to compute the effective radius $R_{\chi,\text{eff}}$ in Eq. (3) if $\tau_0 > \tau_{0,\text{min}}$ in Eq. (4) so that $R_{\chi,\text{min}}$ is real and non-zero. The right panel of Fig. 3 demonstrates how constraints on f_{DM} would look for fixed physical clump sizes. The constraints cut off suddenly for low values of M_χ due to the optical depth's

dependence on clump mass, $\tau_0 \propto M_\chi$, given in Eq. (11). When M_χ is large enough the clumps become opaque and $R_{\chi,\text{eff}} \approx R_\chi$. Conversely, decreasing M_χ drives down the implied optical depth τ_0 . As is apparent in Eq. (3) the effective radius quickly becomes zero once the required optical depth τ_0 becomes too large. The lower mass cut-off arises due to $\tau_0 \approx \tau_{0,\text{min}}$, so that

$$M_{\chi,\text{min}} = \frac{2\pi m_\chi R_\chi^2 \ln(1 - \mu_0)}{3\sigma}. \quad (12)$$

Hence the minimum observable clump mass is determined by the minimum amount of dimming required for an event observation. To demonstrate this dependence, the purple (lime green) curves in the right panel of Fig. 3 show the effect of requiring a smaller dimming threshold of $\mu_0 = 0.34$ ($\mu_0 = 0.01$).

Note that in Fig. 3 we assume that there would be no candidate dimming events in the indicated surveys, for a light dimming of a factor $\mu_0 = 0.34$ (where the brightening event threshold in microlensing surveys is similarly 0.34). We stress that the dimming analysis has not yet been undertaken. It will require a foreground analysis of the expected number of dimming events from non-DM astrophysical events. In this work we assume that no candidate dimming events have been found in the data for our estimates, and leave a more careful study of the individual light curves in the data for a future

study. In addition, while we have overlaid microlensing constraints from point lenses in Fig. 3, we comment that for extended DM objects which are large enough, the constraints on f_{DM} can vary drastically depending on the assumed density profile of the object. In general, microlensing constraints get weaker as the object becomes less dense [41]. Therefore to compare the possible constraints from dimming, we have only shown the microlensing constraints from point-like lenses.

IV. CONSTRAINTS ON DARK MATTER MICROPHYSICS

While in the previous section we have considered the relationship between the number of expected dimming events as a function of the macroscopic properties of the DM clumps, in this section we show how dimming effects due to DM clumps can be used to constrain the microscopic properties of DM. This is explicitly detailed for elastic DM-SM photon scattering and for millicharged dark matter.

A. Dark matter–photon elastic scattering

To apply the DM clump dimming analysis to more specific dark matter models, we first recast constraints shown in Fig. 3 into limits on a photon interaction cross section in terms of the mass of the DM particle for a fixed fraction of dark matter in clumps, f_{DM} . By considering dimming due to elastic scattering $\chi\gamma \rightarrow \chi\gamma$ between DM particles and SM photons, Fig. 4 shows how the null observation of dimming events in OGLE-III+IV would place constraints in $m_\chi - \sigma_{\chi\gamma}$ parameter space. The top panels correspond to a fixed optical depth of $\tau_0 = 1$ which in turn implies an effective radius of $R_{\chi,\text{eff}} \approx R_\chi$. We show in orange (blue) constraints assuming $f_{\text{DM}} = 1$ ($f_{\text{DM}} = 0.1$) fraction of DM in compact objects at fixed masses of $M_\chi = 10^{-2}M_\odot$ in the left panel and $M_\chi = 10^0M_\odot$ in the right panel. The constraints fall off at low values of dark matter mass m_χ and high values of $\sigma_{\chi\gamma}$ because these would result in smaller DM clump sizes (for fixed optical depth), which would avoid detection in the microlensing surveys as they are limited by the minimum event time $t_{E,\text{min}}$. On the other side of the sensitivity band, for lower values of m_χ and higher values of $\sigma_{\chi\gamma}$, the constraints get weaker since the sizes of the objects would be too large and are therefore limited by the maximum event time $t_{E,\text{max}}$.

Given a value of m_χ and $\sigma_{\chi\gamma}$, rather than requiring that the characteristic optical depth τ_0 is fixed, we can instead fix the physical size of the clumps R_χ , and solve for τ_0 in Eq. (15) as discussed for the right panel of Fig. 3. The bottom panels of Fig. 4 show possible constraints on m_χ and $\sigma_{\chi\gamma}$ assuming various fixed physical radii for clump masses of $M_\chi = 10^{-2}M_\odot$ in the left panel and $M_\chi = 10^0M_\odot$ in the right panel. Similar to the top pan-

els of Fig. 4 discussed previously, the high- m_χ , low- $\sigma_{\chi\gamma}$ behaviour of the constraints is due to the DM objects becoming too small for detection. Note that at a fixed clump radius, considering a more massive object generally results in stronger bounds. This can be seen in the $R_\chi = 10^2R_\odot$ region in the bottom two panels of Fig. 4. However, since $N_{\text{events}} \propto M_\chi^{-1}$ in the high clump mass limit, these constraints eventually vanish below N_{thresh} – which can be seen below the $R_\chi = 10R_\odot$ lines in the bottom panels.

In all panels of Fig. 4, we have plotted constraints on $\sigma_{\chi\gamma}$ from analyses of Planck and baryonic acoustic oscillation (BAO) data [54], as well as constraints from considering the population of MW satellites [55]. However, we note that these constraints have assumed that all of dark matter is able to interact with the SM photon, and are thus expected to get weaker as the fraction of DM permitted to interact with SM photons decrease. Therefore in the case that the χ particles responsible for dimming are a subdominant component of DM, dimming effects could provide competitive bounds for $m_\chi > 10^{-3}$ GeV. The behaviour of the existing constraints [54, 55] as one reduces f_{DM} , are not currently known. Furthermore, if all of the χ reside in compact objects, then DM photon-scattering causing small scale DM structures to wash out, which is the effect considered in Ref. [55], requires further consideration.

B. Millicharged dark matter

Next we demonstrate how the lampshade effect can be used to search for a specific dark matter model in clumps. We consider a simple, asymmetric dark sector, comprised of a dark Dirac fermion χ with mass m_χ and a light dark photon V_μ with mass $m_{\gamma'}$, which kinetically mixes with the standard model photon A_μ . The relevant terms in the Lagrangian are then

$$\mathcal{L} \supset \bar{\chi}(i\gamma^\mu D_\mu - m_\chi)\chi - \frac{1}{4}V_{\mu\nu}V^{\mu\nu} - \frac{1}{2}m_{\gamma'}^2V_\mu V^\mu - \frac{\epsilon}{2}V_{\mu\nu}F^{\mu\nu}, \quad (13)$$

where $F_{\mu\nu} = \partial_\mu A_\nu - \partial_\nu A_\mu$ is the usual field strength tensor for the standard model photon and $V_{\mu\nu}$ is similarly defined for the dark photon, so the last term in Eq. (13) is a kinetic mixing term with a kinetic mixing parameter ϵ . $D_\mu = \partial_\mu - ig_D V_\mu$ is the covariant derivative with $\alpha_D = g_D^2/(4\pi)$. This mixing results in the χ particles acquiring a small effective SM electric charge, $q_\chi = \epsilon g_D/e$, where e is the SM electromagnetic coupling. We note that given present bounds, for a sufficiently light dark photon, the mixing parameter ϵ can have values approaching unity, *e.g.* [71, 72]. This class of models, called millicharged particles [47], has been widely studied both as a BSM particle and a DM candidate (see, *e.g.* [73–79]).

For a clump of millicharged χ particles, SM photons emitted from a source star can undergo Compton

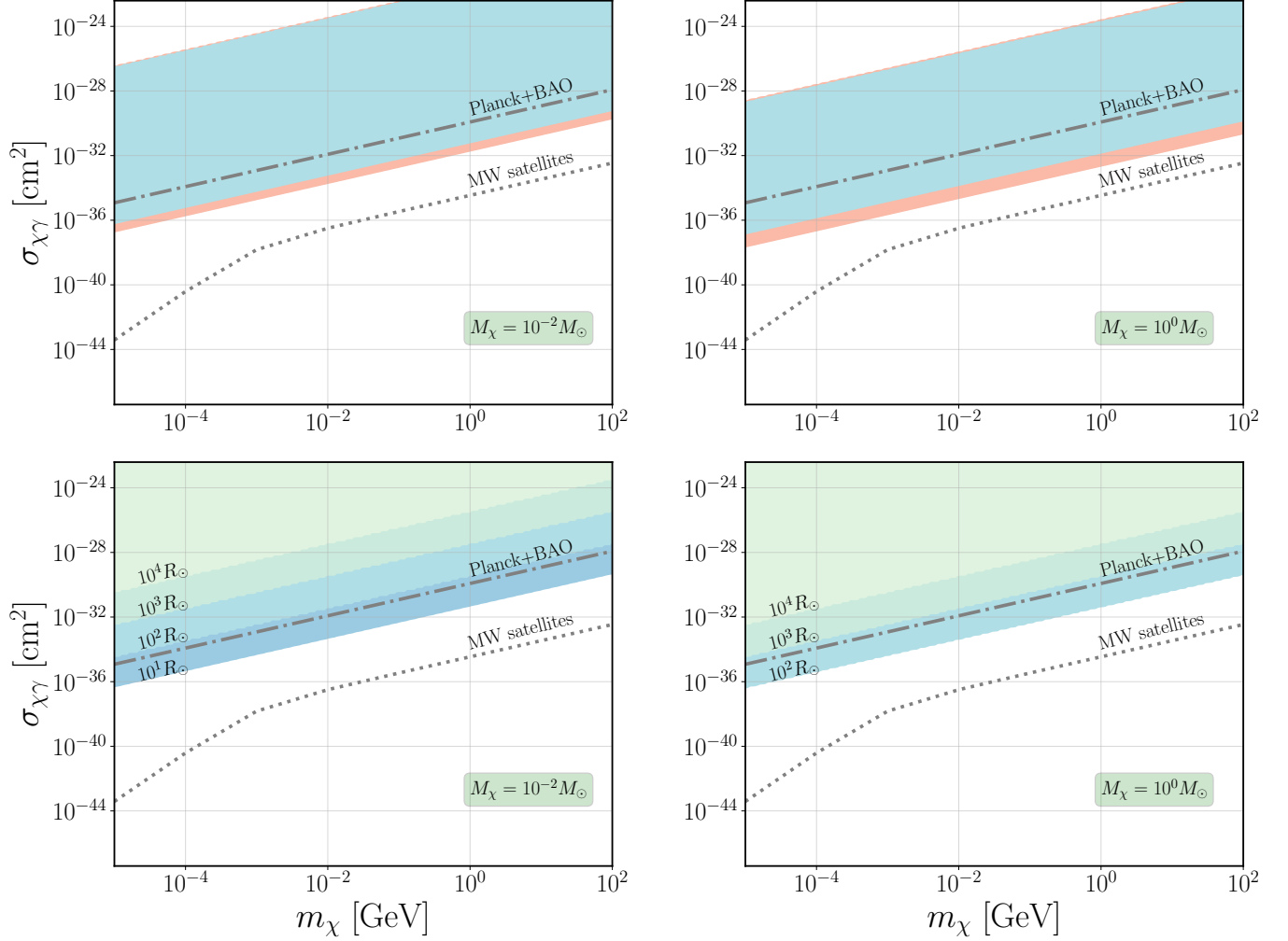


FIG. 4. Constraints that could be placed on m_χ and $\sigma_{\chi\gamma}$ for elastic scattering of SM photons and χ -particles from a future null analysis of dimming events in the OGLE-III+IV surveys. **Top panels:** Constraints at a fixed characteristic depth $\tau_0 = 1$, where the orange (blue) shaded regions are constraints, assuming that $f_{\text{DM}} = 1$ ($f_{\text{DM}} = 0.1$) of DM is inside of clumps of masses $M_\chi = 10^{-2}M_\odot$ in the left panel and $M_\chi = 10^0M_\odot$ in the right panel. **Bottom panels:** Constraints at fixed physical sizes R_χ between 10 to 10^4R_\odot , and masses $M_\chi = 10^{-2}M_\odot$ in the left panel and $M_\chi = 10^0M_\odot$ in the right panel, assuming these objects make up $f_{\text{DM}} = 0.1$ of the dark matter. In all panels, the overlaid gray dashed-dotted line are bounds on the elastic scattering cross section from Planck+BAO [54], while the gray dotted line are bounds from MW satellite galaxies [55]. We note the MW satellite constraints are calculated for $f_{\text{DM}} = 1$ and for dark matter that has not formed structures such as those considered in this work, causing them to likely be quite different for the scenarios covered in this paper.

scattering-like processes with the χ particles. In the case of dimming, since we are only interested in the deficit of SM photons, we are interested in both processes $\chi\gamma \rightarrow \chi\gamma$ and $\chi\gamma \rightarrow \chi\gamma'$. In the case of $\chi\gamma \rightarrow \chi\gamma$, the SM photon would scatter with the cloud of χ -particles, resulting in an angular deflection in the original path of the SM photon. However, this process is of order $\mathcal{O}(\epsilon^4)$, while the $\chi\gamma \rightarrow \chi\gamma'$ is of order $\mathcal{O}(\epsilon^2)$. Hence we only consider the dominant process for dimming, $\chi\gamma \rightarrow \chi\gamma'$, in our analysis. In the low energy limit, the cross section for this is simply the Thomson cross section multiplied by factors

of the kinetic mixing parameter,

$$\sigma = \frac{8\pi\alpha_D^2\epsilon^2}{3m_\chi^2}. \quad (14)$$

In this model, the relationship between the model parameters and the physical quantities of the DM cloud is given by

$$R_\chi = \sqrt{\frac{2\alpha_D^2\epsilon^2 M_\chi}{m_\chi^3\tau_0}}. \quad (15)$$

Fig. 5 shows constraints that could be placed on m_χ and q_χ from the null observation of DM dimming events

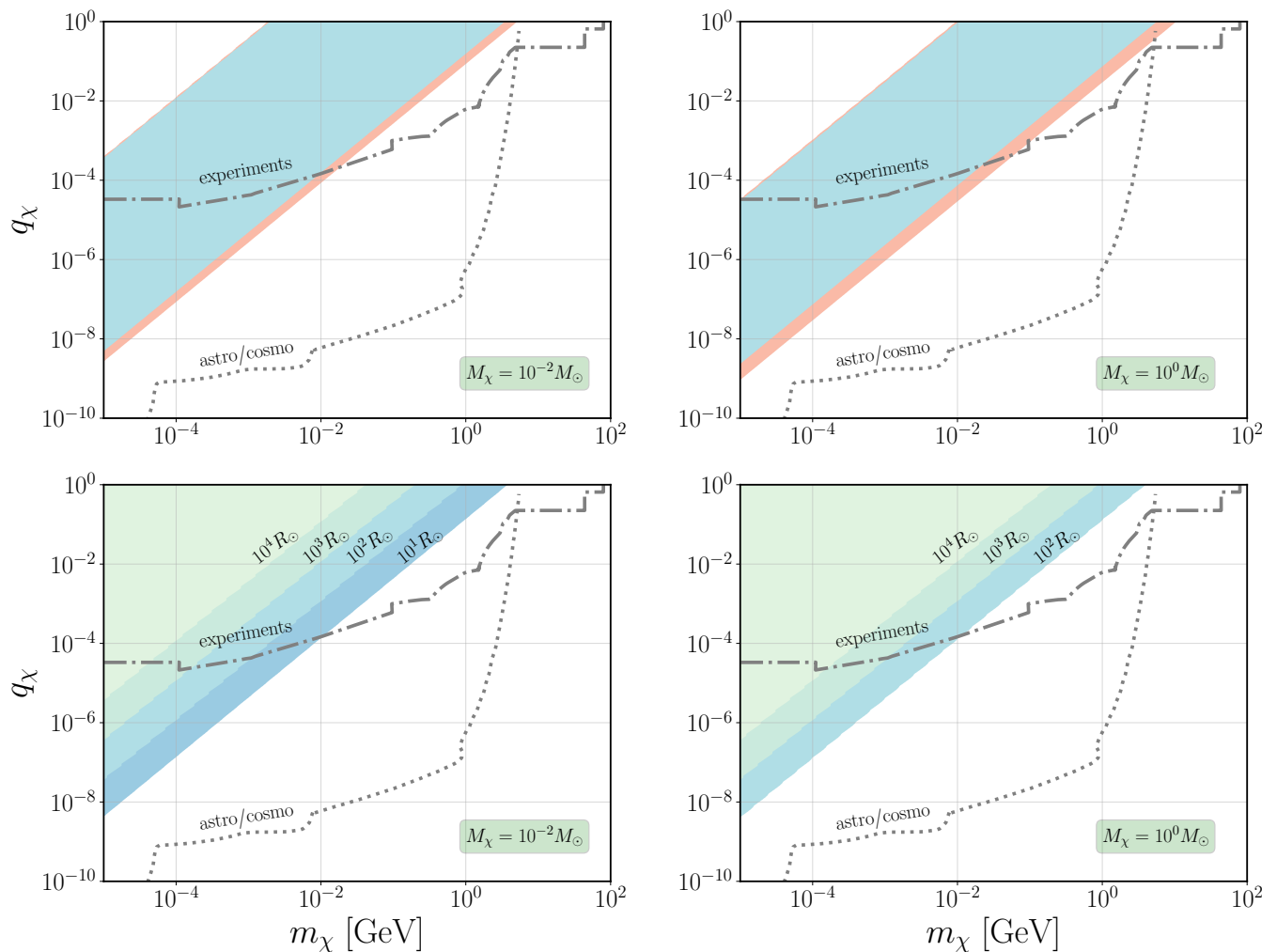


FIG. 5. Constraints on the millicharged particle mass m_χ and effective fractional charge q_χ from null observations of dimming events in OGLE-III+IV, similar to Fig. 4. **Top panels:** Constraints at varying physical clump sizes and a fixed characteristic depth $\tau_0 = 1$, where the orange (blue) shaded regions are constraints, assuming that $f_{\text{DM}} = 1$ ($f_{\text{DM}} = 0.01$) of DM is inside of clumps of masses $M_\chi = 10^{-2} M_\odot$ in the left panel and $M_\chi = 10^0 M_\odot$ in the right panel. **Bottom panels:** Constraints at varying optical depths and fixed physical sizes R_χ from 10 to $10^4 R_\odot$. Overlaid dotted lines labelled astro/cosmo correspond to a combination of constraints from SN1987A [56], stellar evolution [57, 58], and limits on ΔN_{eff} from BBN and CMB [57, 59]. Overlaid dotted-dashed lines correspond to constraints from a variety of experiments, including colliders [60], SLAC [61], OPOS [62], ArgoNeuT [63], BEBC [64] and milliQan [65]. There are also constraints on millicharged DM from interstellar gas cloud cooling [66–70], which will depend on future modeling of millicharged clumps heating local portions of gas clouds.

from OGLE-III+IV, assuming $\alpha_D = 0.1$. All panels and their behaviour are similar to Fig. 4, described above. We have also overlaid constraints on millicharged particles from astrophysical/cosmological considerations such as SN1987A [56], stellar evolution of horizontal branch stars, red giants, and white dwarfs [57, 58], and limits on ΔN_{eff} from big bang nucleosynthesis (BBN) and the cosmic microwave background (CMB) [57, 59], as well as from experiments, comprised of a combination of constraints from colliders [60], SLAC [61], OPOS [62], ArgoNeuT [63], BEBC [64] and milliQan [65]. There are also constraints on millicharged DM in this region of parameter space from interstellar gas cloud cooling [66–70], which will depend non-trivially on the modeling of

millicharged clumps heating local portions of gas clouds. Note that we have not shown the constraint obtained by requiring that the DM-baryon fluid at recombination is completely decoupled [80], as this is a stronger cosmological condition than necessary.

While we have assumed that parameters in the event rate expressions Eqs. (7) and (8) for dimming events were similar to those of microlensing, different parameters can lead to higher sensitivities (and therefore stronger constraints). In particular, while the minimum event time for microlensing in OGLE-III+IV was $t_{E,\text{min}} = 1$ day [49, 50], if the efficiency for dimming effects was permitted to be non-zero at lower event times, then the surveys would be sensitive to smaller sizes. Note that, a

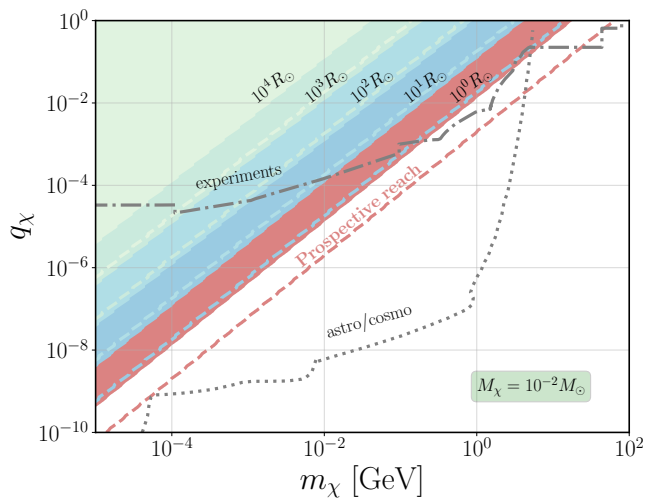


FIG. 6. Same as bottom-left panel of Fig. 5, except assuming a minimum event time of $t_{E,\min} = 0.01$ days. The shaded regions assume a dimming fraction of $\mu_0 = 0.34$ while the dashed lines assume a lower dimming of $\mu_0 = 0.01$ for the same color. We have indicated in red the constraints for a prospective reach, where due to the smaller minimum event time we are more sensitive to smaller objects. All other shaded regions remain unchanged from the bottom-left panel of Fig. 5. Only m_χ and q_χ are varied between the curves, with $\alpha_D = 0.1$. Overlaid dotted lines labelled astro/cosmo correspond to a combination of constraints from SN1987A [56], stellar evolution [57, 58], and limits on ΔN_{eff} from BBN and CMB [57, 59]. Overlaid dotted-dashed lines correspond to constraints from a variety of experiments, including colliders [60], SLAC [61], OPOS [62], ArgoNeuT [63], BEBC [64] and milliQan [65].

lower minimum event time even for the case of microlensing is considered in other surveys, such as Subaru/HSC and the future Roman telescope, in which previous works have considered a minimum event time of 2 minutes [42] and 15 minutes [81, 82], respectively. Additionally, if the threshold for a minimum amount of dimming was lower rather than the fraction of $\mu_0 = 0.34$ (which was chosen to mirror the amplification factor for microlensing), then the surveys could be more sensitive to more dilute DM clumps. A lower threshold for dimming can be feasible since OGLE can be sensitive at the milli-magnitude level [38].

To demonstrate these effects, Fig. 6 shows limits on m_χ and q_χ assuming a lower minimum event time of $t_{E,\min} = 0.01$ days for two different dimming thresholds. The shaded areas correspond to a dimming of $\mu_0 = 0.34$, while the dashed lines correspond to a dimming of $\mu_0 = 0.01$. Comparing between the bottom-left panel of Fig. 5 and Fig. 6, we see that considering a shorter minimum event time does not change the reach of the constraints at clump sizes which would already have created observable dimming for a higher minimum event time. Instead, a shorter minimum event time renders surveys sensitive to smaller clump sizes, since smaller clumps

imply shorter dimming episodes during their transit in front of stars.

On the other hand, decreasing the required amount of dimming from $\mu_0 = 0.34$ to $\mu_0 = 0.01$ (shown as dashed lines in Fig. 6) is advantageous because for a given clump size, since dimming events from clumps are then observable at higher values of the DM mass m_χ and lower values of the charge q_χ . This is because the required optical depth of the clump, $\tau_{0,\min}$, is smaller for a smaller dimming sensitivity threshold. We here reiterate that a threshold of $\mu_0 = 0.01$ is obtainable, for instance, in OGLE-IV as it can be sensitive to changes in brightness at the milli-magnitude level for the brightest stars [38].

Hence the strongest bounds arise when we consider both a lower minimum event time and a lower threshold for a dimming event, which yields sensitivity to the smallest clump sizes and largest effective radii. For the case of solar-radius-size clumps, with sizes $R_\chi = 10^0 R_\odot$ with a minimum event time of $t_{E,\min} = 0.01$ days and a dimming threshold of $\mu_0 = 0.01$ (the right-most dashed line in Fig. 6), we see null observations of dimming events would compete with other bounds for millicharged particles at both $m_\chi \approx 10^{-4}$ GeV and $m_\chi \approx 10$ GeV.

V. CONCLUSION

In this work, we have shown how existing microlensing surveys can observe dimming of distant stars due to clouds of DM that interact with photons passing through the line of sight to the stars. We have shown that dimming effects are generally more sensitive than microlensing events for larger sized DM clumps (*c.f.* [42]) because microlensing is limited by the maximum Einstein radius of the object. The null observation of dimming effects in microlensing surveys such like EROS-2 and OGLE-III+IV could be used to search for DM clumps, and could even be used to determine their size, mass, and contribution to the DM density, as well as microphysical properties of DM, such as the mass of the DM particle, DM-photon interaction cross sections, and the effective charge of the DM particle in a millicharged DM scenario. These searches are complementary or competitive with existing DM-photon interaction searches, depending on the survey observing cadence and sensitivity to changes in source brightness. We emphasize that the majority of our analysis was performed model-independently. This approach could be used to look for or constrain any dark sector model that interacts with photons and forms compact objects. Searches for dimming events can be undertaken using existing/upcoming microlensing data, without requiring any additional hardware or equipment.

We bring the reader's attention to several possible extensions to our treatment. First, in this work, we have only considered the effects of dimming due to the optical thickness of the intervening dark matter clump. However, for dark matter clumps with densities in an intersecting

region of sensitivity (*c.f.* Fig. 1), the clump not only acts as a lampshade, but also a gravitational lens. In this case, the dimming and brightening of star light are competing effects, which could result in a lower number of events when considering either microlensing or dimming. In this case, there are additional signatures to look for, *e.g.* the expected brightness may shift up, then down when the line-of-sight crosses the Einstein radius and then the physical clump radius. Second, while in this work we have considered constant density profiles for the DM lampshades, we note that different density profiles can change the bound set on the amount of dark matter in clumps f_{DM} (see Refs. [41, 42] for the effects of density profiles on f_{DM} in the case of microlensing). Furthermore, our analysis was performed assuming that the source star can be treated as a point source. However, the source can also be considered as an extended object (see *e.g.* Refs. [42, 81–83]), which is relevant for surveys such as Subaru/HSC and the future Roman Space Telescope which are able to resolve the source star. These surveys can also lead to lower minimum observation times and higher sensitivities to changes in brightness, which

we expect will strengthen the bounds one can place from dimming effects. Finally, we note that considering light from an extended source should increase survey dimming event sensitivity, making a study of dimming effects for extended sources in these surveys a clear next step.

ACKNOWLEDGMENTS

We thank Christopher V. Cappiello, Wendy Crumrine, Audrey Fung, Vera Gluscevic, Przemek Mróz, Nirmal Raj, and Han Wu for useful discussions. The authors and this work were supported by the Arthur B. McDonald Canadian Astroparticle Physics Research Institute, the Natural Sciences and Engineering Research Council of Canada (NSERC), and the Canada Foundation for Innovation. Research at Perimeter Institute is supported by the Government of Canada through the Department of Innovation, Science, and Economic Development, and by the Province of Ontario. JLK is supported by an NSERC Canada Graduate Scholarship - Doctoral (CGS-D).

-
- [1] S. Hawking, Gravitationally collapsed objects of very low mass, *Mon. Not. Roy. Astron. Soc.* **152**, 75 (1971).
- [2] B. J. Carr and S. W. Hawking, Black holes in the early Universe, *Mon. Not. Roy. Astron. Soc.* **168**, 399 (1974).
- [3] B. Carr, F. Kuhnel, and M. Sandstad, Primordial Black Holes as Dark Matter, *Phys. Rev. D* **94**, 083504 (2016), [arXiv:1607.06077 \[astro-ph.CO\]](#).
- [4] A. M. Green and B. J. Kavanagh, Primordial Black Holes as a dark matter candidate, *J. Phys. G* **48**, 043001 (2021), [arXiv:2007.10722 \[astro-ph.CO\]](#).
- [5] P. Villanueva-Domingo, O. Mena, and S. Palomares-Ruiz, A brief review on primordial black holes as dark matter, *Front. Astron. Space Sci.* **8**, 87 (2021), [arXiv:2103.12087 \[astro-ph.CO\]](#).
- [6] C. Kouvaris and N. G. Nielsen, Asymmetric Dark Matter Stars, *Phys. Rev. D* **92**, 063526 (2015), [arXiv:1507.00959 \[hep-ph\]](#).
- [7] J. Eby, C. Kouvaris, N. G. Nielsen, and L. C. R. Wijewardhana, Boson Stars from Self-Interacting Dark Matter, *JHEP* **02**, 028, [arXiv:1511.04474 \[hep-ph\]](#).
- [8] A. Maselli, P. Pnigouras, N. G. Nielsen, C. Kouvaris, and K. D. Kokkotas, Dark stars: gravitational and electromagnetic observables, *Phys. Rev. D* **96**, 023005 (2017), [arXiv:1704.07286 \[astro-ph.HE\]](#).
- [9] L. Amendola, J. Rubio, and C. Wetterich, Primordial black holes from fifth forces, *Phys. Rev. D* **97**, 081302 (2018), [arXiv:1711.09915 \[astro-ph.CO\]](#).
- [10] M. I. Gresham, H. K. Lou, and K. M. Zurek, Early Universe synthesis of asymmetric dark matter nuggets, *Phys. Rev. D* **97**, 036003 (2018), [arXiv:1707.02316 \[hep-ph\]](#).
- [11] J. H. Chang, D. Egana-Ugrinovic, R. Essig, and C. Kouvaris, Structure Formation and Exotic Compact Objects in a Dissipative Dark Sector, *JCAP* **03**, 036, [arXiv:1812.07000 \[hep-ph\]](#).
- [12] S. Savastano, L. Amendola, J. Rubio, and C. Wetterich, Primordial dark matter halos from fifth forces, *Phys. Rev. D* **100**, 083518 (2019), [arXiv:1906.05300 \[astro-ph.CO\]](#).
- [13] M. M. Flores and A. Kusenko, Primordial Black Holes from Long-Range Scalar Forces and Scalar Radiative Cooling, *Phys. Rev. Lett.* **126**, 041101 (2021), [arXiv:2008.12456 \[astro-ph.CO\]](#).
- [14] J. Gurian, D. Jeong, M. Ryan, and S. Shandera, Molecular Chemistry for Dark Matter II: Recombination, Molecule Formation, and Halo Mass Function in Atomic Dark Matter, *Astrophys. J.* **934**, 121 (2022), [arXiv:2110.11964 \[astro-ph.CO\]](#).
- [15] M. Hippert, J. Setford, H. Tan, D. Curtin, J. Noronha-Hostler, and N. Yunes, Mirror neutron stars, *Phys. Rev. D* **106**, 035025 (2022), [arXiv:2103.01965 \[astro-ph.HE\]](#).
- [16] M. M. Flores, A. Kusenko, L. Pearce, and G. White, Fireball baryogenesis from early structure formation due to Yukawa forces, *Phys. Rev. D* **108**, L091705 (2023), [arXiv:2208.09789 \[hep-ph\]](#).
- [17] J. Gurian, M. Ryan, S. Schon, D. Jeong, and S. Shandera, A Lower Bound on the Mass of Compact Objects from Dissipative Dark Matter, *Astrophys. J. Lett.* **939**, L12 (2022), [Erratum: *Astrophys. J. Lett.* 949, L44 (2023), Erratum: *Astrophys. J.* 949, L44 (2023)], [arXiv:2209.00064 \[astro-ph.CO\]](#).
- [18] G. Domènech, D. Inman, A. Kusenko, and M. Sasaki, Halo formation from Yukawa forces in the very early Universe, *Phys. Rev. D* **108**, 103543 (2023), [arXiv:2304.13053 \[astro-ph.CO\]](#).
- [19] M. M. Flores, Y. Lu, and A. Kusenko, Structure formation after reheating: Supermassive primordial black holes and Fermi ball dark matter, *Phys. Rev. D* **108**, 123511 (2023), [arXiv:2308.09094 \[astro-ph.CO\]](#).
- [20] S. Roy, X. Shen, M. Lisanti, D. Curtin, N. Murray, and P. F. Hopkins, Simulating Atomic Dark Matter in Milky Way Analogs, *Astrophys. J. Lett.* **954**, L40 (2023),

- arXiv:2304.09878 [astro-ph.GA].
- [21] C. Gemmill, S. Roy, X. Shen, D. Curtin, M. Lisanti, N. Murray, and P. F. Hopkins, Dissipative Dark Substructure: The Consequences of Atomic Dark Matter on Milky Way Analog Subhalos, *Astrophys. J.* **967**, 21 (2024), arXiv:2311.02148 [astro-ph.GA].
- [22] J. Bramante, M. Diamond, and J. L. Kim, The effect of multiple cooling channels on the formation of dark compact objects, *JCAP* **02**, 002, arXiv:2309.13148 [hep-ph].
- [23] J. Bramante, C. V. Cappiello, M. D. Diamond, J. L. Kim, Q. Liu, and A. C. Vincent, Dissipative dark cosmology: From early matter dominance to delayed compact objects, *Phys. Rev. D* **110**, 043041 (2024), arXiv:2405.04575 [hep-ph].
- [24] S. Roy, X. Shen, J. Barron, M. Lisanti, D. Curtin, N. Murray, and P. F. Hopkins, Aggressively-Dissipative Dark Dwarfs: The Effects of Atomic Dark Matter on the Inner Densities of Isolated Dwarf Galaxies, arXiv:2408.15317 [astro-ph.GA] (2024).
- [25] G. F. Giudice, M. McCullough, and A. Urbano, Hunting for Dark Particles with Gravitational Waves, *JCAP* **10**, 001, arXiv:1605.01209 [hep-ph].
- [26] J. A. Dror, H. Ramani, T. Trickle, and K. M. Zurek, Pulsar Timing Probes of Primordial Black Holes and Subhalos, *Phys. Rev. D* **100**, 023003 (2019), arXiv:1901.04490 [astro-ph.CO].
- [27] Y. Bai, A. J. Long, and S. Lu, Tests of Dark MACHOs: Lensing, Accretion, and Glow, *JCAP* **09**, 044, arXiv:2003.13182 [astro-ph.CO].
- [28] D. Croon, S. Ipek, and D. McKeen, Gravitational wave constraints on extended dark matter structures, *Phys. Rev. D* **107**, 063012 (2023), arXiv:2205.15396 [astro-ph.CO].
- [29] I. Armstrong, B. Gurbuz, D. Curtin, and C. D. Matzner, Electromagnetic Signatures of Mirror Stars, *Astrophys. J.* **965**, 42 (2024), arXiv:2311.18086 [astro-ph.HE].
- [30] H. Banks, D. M. Grabowska, and M. McCullough, Gravitational wave backgrounds from colliding exotic compact objects, *Phys. Rev. D* **108**, 035017 (2023), arXiv:2302.07887 [gr-qc].
- [31] N. Raj, Supernovae and superbursts triggered by dark matter clumps, *Phys. Rev. D* **109**, 123020 (2024), arXiv:2306.14981 [hep-ph].
- [32] T. X. Tran, S. R. Geller, B. V. Lehmann, and D. I. Kaiser, Close encounters of the primordial kind: a new observable for primordial black holes as dark matter, arXiv:2312.17217 [astro-ph.CO] (2023).
- [33] J. B. Dent, B. Dutta, and T. Xu, Multi-messenger Probes of Asteroid Mass Primordial Black Holes: Superradiance Spectroscopy, Hawking Radiation, and Microlensing, arXiv:2404.02956 [hep-ph] (2024).
- [34] D. E. Kaplan, X. Luo, N. H. Nguyen, S. Rajendran, and E. H. Tanin, Indirect Searches for Ultraheavy Dark Matter in the Time Domain, arXiv:2407.06262 [hep-ph] (2024).
- [35] B. Paczynski, Gravitational Microlensing by the Galactic Halo, *ApJ* **304**, 1 (1986).
- [36] P. Tisserand *et al.* (EROS-2), Limits on the Macho Content of the Galactic Halo from the EROS-2 Survey of the Magellanic Clouds, *Astron. Astrophys.* **469**, 387 (2007), arXiv:astro-ph/0607207.
- [37] A. Udalski, The Optical Gravitational Lensing Experiment. Real Time Data Analysis Systems in the OGLE-III Survey, *Acta Astron.* **53**, 291 (2003), arXiv:astro-ph/0401123 [astro-ph].
- [38] A. Udalski, M. K. Szymański, and G. Szymański, OGLE-IV: Fourth Phase of the Optical Gravitational Lensing Experiment, *Acta Astron.* **65**, 1 (2015), arXiv:1504.05966 [astro-ph.SR].
- [39] H. Niikura *et al.*, Microlensing constraints on primordial black holes with Subaru/HSC Andromeda observations, *Nature Astron.* **3**, 524 (2019), arXiv:1701.02151 [astro-ph.CO].
- [40] B. Carr, K. Kohri, Y. Sendouda, and J. Yokoyama, Constraints on primordial black holes, *Reports on Progress in Physics* **84**, 116902 (2021).
- [41] D. Croon, D. McKeen, and N. Raj, Gravitational microlensing by dark matter in extended structures, *Phys. Rev. D* **101**, 083013 (2020), arXiv:2002.08962 [astro-ph.CO].
- [42] D. Croon, D. McKeen, N. Raj, and Z. Wang, Subaru-HSC through a different lens: Microlensing by extended dark matter structures, *Phys. Rev. D* **102**, 083021 (2020), arXiv:2007.12697 [astro-ph.CO].
- [43] D. Croon and S. Sevillano Muñoz, Repository for extended dark matter object constraints, arXiv:2407.02573 [astro-ph.CO] (2024).
- [44] Y. Bai, S. Lu, and N. Orlofsky, Dark exoplanets, *Phys. Rev. D* **108**, 103026 (2023), arXiv:2303.12129 [astro-ph.EP].
- [45] K. Griest, Galactic Microlensing as a Method of Detecting Massive Compact Halo Objects, *Astrophys. J.* **366**, 412 (1991).
- [46] C. Alcock *et al.* (MACHO), The MACHO project first year LMC results: The Microlensing rate and the nature of the galactic dark halo, *Astrophys. J.* **461**, 84 (1996), arXiv:astro-ph/9506113.
- [47] B. Holdom, Two U(1)'s and Epsilon Charge Shifts, *Phys. Lett. B* **166**, 196 (1986).
- [48] H. Niikura, M. Takada, S. Yokoyama, T. Sumi, and S. Masaki, Constraints on Earth-mass primordial black holes from OGLE 5-year microlensing events, *Phys. Rev. D* **99**, 083503 (2019), arXiv:1901.07120 [astro-ph.CO].
- [49] P. Mroz *et al.*, No massive black holes in the Milky Way halo, arXiv:2403.02386 [astro-ph.GA] (2024).
- [50] P. Mróz *et al.*, Microlensing Optical Depth and Event Rate toward the Large Magellanic Cloud Based on 20 yr of OGLE Observations, *Astrophys. J. Suppl.* **273**, 4 (2024), arXiv:2403.02398 [astro-ph.GA].
- [51] M. Wenger *et al.*, The simbad astronomical database, *Astron. Astrophys. Suppl. Ser.* **143**, 9 (2000), arXiv:astro-ph/0002110.
- [52] M. Cirelli, G. Corcella, A. Hektor, G. Hutsi, M. Kadastik, P. Panci, M. Raidal, F. Sala, and A. Strumia, PPPC 4 DM ID: A Poor Particle Physicist Cookbook for Dark Matter Indirect Detection, *JCAP* **03**, 051, [Erratum: *JCAP* **10**, E01 (2012)], arXiv:1012.4515 [hep-ph].
- [53] P. Mróz, A. Udalski, J. Skowron, M. K. Szymański, I. Soszyński, L. Wyrzykowski, P. Pietrukowicz, S. Kozłowski, R. Poleski, K. Ulaczyk, K. Rybicki, and P. Iwanek, Microlensing Optical Depth and Event Rate toward the Galactic Bulge from 8 yr of OGLE-IV Observations, *ApJS* **244**, 29 (2019), arXiv:1906.02210 [astro-ph.SR].
- [54] N. Becker, D. C. Hooper, F. Kahlhoefer, J. Lesgourgues, and N. Schöneberg, Cosmological constraints on multi-interacting dark matter, *JCAP* **02**, 019, arXiv:2010.04074

- [astro-ph.CO].
- [55] W. Crumrine, E. O. Nadler, R. An, and V. Gluscevic, Dark Matter Coupled to Radiation: Limits from the Milky Way Satellites, [arXiv:2406.19458 \[astro-ph.CO\]](#) (2024).
- [56] J. H. Chang, R. Essig, and S. D. McDermott, Supernova 1987A Constraints on Sub-GeV Dark Sectors, Millicharged Particles, the QCD Axion, and an Axion-like Particle, *JHEP* **09**, 051, [arXiv:1803.00993 \[hep-ph\]](#).
- [57] H. Vogel and J. Redondo, Dark Radiation constraints on minicharged particles in models with a hidden photon, *JCAP* **02**, 029, [arXiv:1311.2600 \[hep-ph\]](#).
- [58] A. Fung, S. Heeba, Q. Liu, V. Muralidharan, K. Schutz, and A. C. Vincent, New bounds on light millicharged particles from the tip of the red-giant branch, *Phys. Rev. D* **109**, 083011 (2024), [arXiv:2309.06465 \[hep-ph\]](#).
- [59] P. Adshead, P. Ralegankar, and J. Shelton, Dark radiation constraints on portal interactions with hidden sectors, *JCAP* **09**, 056, [arXiv:2206.13530 \[hep-ph\]](#).
- [60] S. Davidson, S. Hannestad, and G. Raffelt, Updated bounds on millicharged particles, *JHEP* **05**, 003, [arXiv:hep-ph/0001179](#).
- [61] A. A. Prinz *et al.*, Search for millicharged particles at SLAC, *Phys. Rev. Lett.* **81**, 1175 (1998), [arXiv:hep-ex/9804008](#).
- [62] A. Badertscher, P. Crivelli, W. Fetscher, U. Gendotti, S. Gninenko, V. Postoev, A. Rubbia, V. Samoylenko, and D. Sillou, An Improved Limit on Invisible Decays of Positronium, *Phys. Rev. D* **75**, 032004 (2007), [arXiv:hep-ex/0609059](#).
- [63] R. Acciarri *et al.* (ArgoNeuT), Improved Limits on Millicharged Particles Using the ArgoNeuT Experiment at Fermilab, *Phys. Rev. Lett.* **124**, 131801 (2020), [arXiv:1911.07996 \[hep-ex\]](#).
- [64] G. Marocco and S. Sarkar, Blast from the past: Constraints on the dark sector from the BEBC WA66 beam dump experiment, *SciPost Phys.* **10**, 043 (2021), [arXiv:2011.08153 \[hep-ph\]](#).
- [65] A. Ball *et al.* (milliQan), Sensitivity to millicharged particles in future proton-proton collisions at the LHC with the milliQan detector, *Phys. Rev. D* **104**, 032002 (2021), [arXiv:2104.07151 \[hep-ex\]](#).
- [66] A. Bhoonah, J. Bramante, F. Elahi, and S. Schon, Calorimetric Dark Matter Detection With Galactic Center Gas Clouds, *Phys. Rev. Lett.* **121**, 131101 (2018), [arXiv:1806.06857 \[hep-ph\]](#).
- [67] A. Bhoonah, J. Bramante, F. Elahi, and S. Schon, Galactic Center gas clouds and novel bounds on ultralight dark photon, vector portal, strongly interacting, composite, and super-heavy dark matter, *Phys. Rev. D* **100**, 023001 (2019), [arXiv:1812.10919 \[hep-ph\]](#).
- [68] A. Bhoonah, J. Bramante, S. Schon, and N. Song, Detecting composite dark matter with long-range and contact interactions in gas clouds, *Phys. Rev. D* **103**, 123026 (2021), [arXiv:2010.07240 \[hep-ph\]](#).
- [69] D. Wadekar and G. R. Farrar, Gas-rich dwarf galaxies as a new probe of dark matter interactions with ordinary matter, *Phys. Rev. D* **103**, 123028 (2021), [arXiv:1903.12190 \[hep-ph\]](#).
- [70] D. Wadekar and Z. Wang, Constraining axion and compact dark matter with interstellar medium heating, *Phys. Rev. D* **107**, 083011 (2023), [arXiv:2211.07668 \[hep-ph\]](#).
- [71] S. Navas *et al.* (Particle Data Group), Review of particle physics, *Phys. Rev. D* **110**, 030001 (2024).
- [72] A. Caputo, A. J. Millar, C. A. J. O’Hare, and E. Vitagliano, Dark photon limits: A handbook, *Phys. Rev. D* **104**, 095029 (2021), [arXiv:2105.04565 \[hep-ph\]](#).
- [73] K. J. Kelly and Y.-D. Tsai, Proton fixed-target scintillation experiment to search for millicharged dark matter, *Phys. Rev. D* **100**, 015043 (2019), [arXiv:1812.03998 \[hep-ph\]](#).
- [74] R. Plestid, V. Takhistov, Y.-D. Tsai, T. Bringmann, A. Kusenko, and M. Pospelov, New Constraints on Millicharged Particles from Cosmic-ray Production, *Phys. Rev. D* **102**, 115032 (2020), [arXiv:2002.11732 \[hep-ph\]](#).
- [75] C. A. Argüelles Delgado, K. J. Kelly, and V. Muñoz Alborno, Millicharged particles from the heavens: single- and multiple-scattering signatures, *JHEP* **11**, 099, [arXiv:2104.13924 \[hep-ph\]](#).
- [76] A. Berlin, J. A. Dror, X. Gan, and J. T. Ruderman, Millicharged relics reveal massless dark photons, *JHEP* **05**, 046, [arXiv:2211.05139 \[hep-ph\]](#).
- [77] X. Gan and Y.-D. Tsai, Cosmic Millicharge Background and Reheating Probes, [arXiv:2308.07951 \[hep-ph\]](#) (2023).
- [78] H. Wu, E. Hardy, and N. Song, Searching for heavy millicharged particles from the atmosphere, [arXiv:2406.01668 \[hep-ph\]](#) (2024).
- [79] A. Berlin and D. Hooper, High-Energy Neutrinos From Millicharged Dark Matter Annihilation in the Sun, [arXiv:2407.04768 \[hep-ph\]](#) (2024).
- [80] S. D. McDermott, H.-B. Yu, and K. M. Zurek, Turning off the Lights: How Dark is Dark Matter?, *Phys. Rev. D* **83**, 063509 (2011), [arXiv:1011.2907 \[hep-ph\]](#).
- [81] W. DeRocco, E. Frangipane, N. Hamer, S. Profumo, and N. Smyth, Revealing terrestrial-mass primordial black holes with the Nancy Grace Roman Space Telescope, *Phys. Rev. D* **109**, 023013 (2024), [arXiv:2311.00751 \[astro-ph.CO\]](#).
- [82] W. DeRocco, N. Smyth, and V. Takhistov, New Light on Dark Extended Lenses with the Roman Space Telescope, *Astrophys. J. Lett.* **965**, L3 (2024), [arXiv:2312.14782 \[astro-ph.CO\]](#).
- [83] H. Winch, J. Setford, J. Bovy, and D. Curtin, Using LSST Microlensing to Constrain Dark Compact Objects in Spherical and Disk Configurations, *Astrophys. J.* **933**, 177 (2022), [arXiv:2012.07136 \[astro-ph.GA\]](#).